

# The Role of Initial Conditions in the Decay of Spatially Periodic Patterns in a Nematic Liquid Crystal

Werner Pesch and Lorenz Kramer

*Institute of Physics, University of Bayreuth, D-95440 Bayreuth, Germany*

Nándor Éber\* and Ágnes Buka

*Research Institute for Solid State Physics and Optics,*

*Hungarian Academy of Sciences, H-1525 Budapest, P.O.B.49, Hungary*

(Dated: February 23, 2006)

## Abstract

The decay of stripe patterns in planarly aligned nematic liquid crystals has been studied experimentally and theoretically. The initial patterns have been generated by the electrohydrodynamic instability and a light diffraction technique has been used to monitor their decay. In our experiments different decay rates have been observed as a function of the pattern wavenumber. According to our theoretical analysis they belong to a spectrum of decay modes and are individually selected in dependence on the initial conditions. Additional insight has emerged from a refined physical optical description of the diffraction intensity. The results compare well with experiments, which include also controlled modifications of the initial conditions to assess different decay modes.

PACS numbers: 47.54.-r, 61.30.Dk, 61.30.Gd, 42.25.Fx

---

\*Electronic address: eber@szfki.hu

## I. INTRODUCTION

The intriguing features of patterns in anisotropic fluids when driven out of equilibrium by an external stress have motivated a wide range of experimental and theoretical studies over the last decades [1]. The most common representatives of uniaxially symmetric fluids are nematic liquid crystals (nematics) which have a locally preferred direction described by the director field  $\mathbf{n}(\mathbf{r}, t)$ .

One of the simplest examples of patterns in nematics is a periodic array of parallel stripes which reflect a periodic modulation of the director and hence that of the optical axis in space. The pattern is often accompanied by material flow in the form of convection rolls and can be induced by various types of excitations like shear flow [2], temperature gradient [3] or electric field [4].

The goal of this work is to investigate the decay of a suitably prepared regular stripe pattern after the driving force has been switched off, i.e. when the system relaxes to the equilibrium (usually homogeneous) ground state. The relaxation time  $\tau$  characterizing the decay process is a key parameter, which reflects the system dynamics. In the theoretical analysis we concentrate on low-amplitude director modulations, either already realized in the initial pattern or reached in the late stage of the decay process. In a recent paper [5] a rigorous theoretical description of the low-amplitude decay process of stripes, characterized by a wavevector  $\mathbf{q}$ , has been presented which is based on the standard equation set of nematohydrodynamics [6, 7]. One arrives at a linear eigenvalue problem, which yields an infinite discrete spectrum of decay rates,  $\mu_i(q)$ , associated with the corresponding eigen (decay) modes  $N_i(z, q)$ . Since only the pattern wavelength,  $\Lambda = \frac{2\pi}{q}$ , and the elastic and viscous material parameters come into play, the analysis of the decay process might also be useful for actually assessing material parameters. Note that the mechanism of producing the patterns influences their subsequent decay only via the initial conditions, which determine the selection of the relevant decay modes.

In our case electroconvection (EC) [4] is used to trigger the initial patterns: an ac voltage is applied to a thin ( $d \sim 10 - 100\mu\text{m}$ ) layer of a planarly oriented, slightly conducting nematic possessing negative dielectric and positive conductivity anisotropies. Varying the easily tunable control parameters (rms voltage  $U$ , circular frequency  $\omega$ , etc.) we place the system into a parameter regime, where periodic stripe (roll) patterns with wavevector  $\mathbf{q}$

parallel to the equilibrium director orientation  $\mathbf{n}_0$  (normal rolls) bifurcate at onset ( $U_c$ ). This state serves as the initial condition for the decay dynamics when the voltage is switched off. Our previous light diffraction measurements of the decay rates for various  $|\mathbf{q}|$  were consistent with the theory and gave the first indications to the selection mechanism of the dominant decay modes [5]. In the present work the analysis will be substantially extended: for a given initial pattern we rigorously determine the individual contributions of the different decay modes to the temporal evolution of the diffraction fringe intensities, which is exploited in the experiment to monitor the decay process.

In Section II we describe briefly the experimental setup and give some background information on the initial EC patterns. Section III is devoted to the linear eigenvalue problem alluded to before, which leads to the decay rate spectrum and in particular to the understanding of the relative importance of the corresponding eigenmodes when the decay from different initial states is considered. In Section IV we present a theoretical analysis of the light diffraction method, where we employ a standard [8, 9] (but refined) physical optical description. In Section V we compare theory and experiment in the linear regime. In addition we show experiments where the initial conditions have been modified either by stronger forcing or by varying the waveform of the driving signal. The paper ends with some concluding remarks and an outlook to future work. An Appendix is devoted to some technical details.

## II. EXPERIMENTAL SETUP

The decay of EC patterns was investigated in standard sandwich cells (E.H.C. Co) which produce by their proper surface treatment a uniform planar orientation of nematics in the equilibrium state. In the experiments we have used the commercial nematic **Phase 5** (Merck) and its factory doped version **Phase 5A**. This substance (a kind of a standard for EC measurements) is chemically stable and its material parameters on which all explicit calculations throughout this paper were based, are well known [10]. All measurements were carried out at the temperature  $T = 30.0 \pm 0.05$  °C kept constant by a PC controlled Instec hot-stage. Cells of different thicknesses  $d$  have been used, where  $d$  was determined by an Ocean Optics spectrophotometer.

The EC instability was typically driven by an ac voltage  $U\sqrt{2}\sin\omega t$  with frequencies

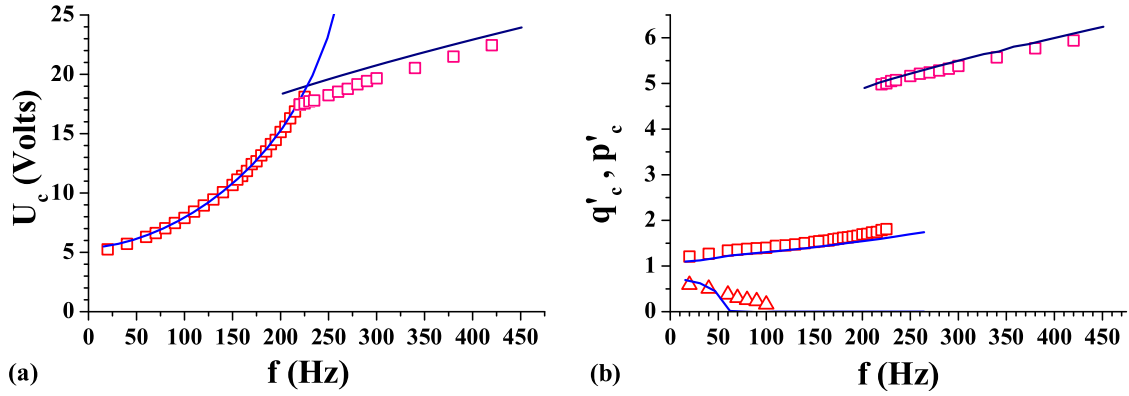


FIG. 1: (a) Critical voltage  $U_c$  and (b) dimensionless components  $q'_c = q_c d / \pi$  (open squares) and  $p'_c = p_c d / \pi$  (open triangles) of the critical wavevector for a **Phase 5** cell ( $d = 9.2 \mu\text{m}$ ) as function of frequency. Measurements (symbols) are compared with theory (solid lines).

$f = \frac{\omega}{2\pi}$  up to 1400 Hz and rms amplitudes  $U$  up to 90 V [11]. Convection in form of rolls with a critical wavevector  $\mathbf{q}_c = (q_c, p_c)$  sets in if the applied voltage  $U$  exceeds the threshold  $U_c(f)$ . In Fig. 1a a typical critical voltage curve is presented as a function of frequency, where the two well known regimes can clearly be identified. At frequencies below the cutoff frequency,  $f_c \approx 225$  Hz, which is material parameter dependent, one observes electroconvection in the *conductive* regime, where the director distortion is practically time independent, whereas it oscillates with  $f$  in the *dielectric* regime above  $f_c$  (for more details see Sect. III). The transition between the two regimes is indicated by a kink of the  $U_c(f)$  curve. In Fig. 1b we show the components  $q_c, p_c$  of the critical wavevector  $\mathbf{q}_c$ . At lower frequencies we have *oblique* rolls with a nonzero angle  $\delta = \arctan(p_c/q_c)$  between  $\mathbf{q}_c$  and  $\mathbf{n}_0$ . Above the Lifshitz frequency,  $f_L \approx 70$  Hz, we have normal rolls with  $p_c = 0$ . At  $f_c$  we observe a jump in  $q_c$ . In Figs. 1a and 1b we have also included the theoretical curves obtained from the linear stability analysis of the nematohydrodynamic equations [4] with the material parameter set for **Phase 5** (see [10] and Table 1 of [5]), which describes the experiments very well.

The cut-off frequency  $f_c$  is proportional to the electrical conductivity of a nematic. **Phase 5** has a low  $f_c = \frac{\omega_c}{2\pi} < 300$  Hz; thus it allows easy measurements of the dielectric EC mode in thin cells. Due to its much higher electrical conductivity **Phase 5A** has a higher cut-off frequency ( $f_c > 1500$  Hz) offering a wide frequency range in the conductive regime, but

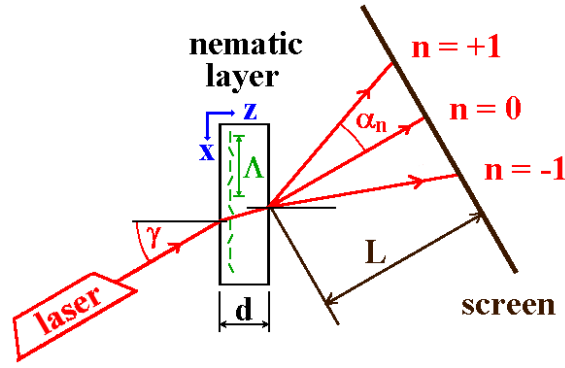


FIG. 2: Schematic sketch of the light diffraction geometry.

makes the dielectric regime inaccessible, since the required voltage becomes too high and would destroy the cells. To facilitate comparison with theory we restricted ourselves to the normal roll regime ( $f > f_L$ ).

While the wavelength  $\Lambda = \frac{2\pi}{q}$  in the conductive regime varies roughly between  $2d$  and  $0.9d$ , in the dielectric regime considerably smaller values  $\approx 0.3d$  become accessible. In order to cover a wide  $q$ -range we have chosen  $d = 28 \mu\text{m}$  for Phase 5A and  $d = 9.2 \mu\text{m}$  for Phase 5, respectively.

The nematic layer (see Fig. 2) is illuminated with a polarized monochromatic laser beam (circular frequency  $\Omega$ , wavelength  $\lambda = \frac{2\pi c}{\Omega} = 650 \text{ nm}$ ,  $c$  is the velocity of light). Diffraction fringes were observed on a screen placed normal to the beam at a distance of  $L = 660 \text{ mm}$ . In order to have a higher contrast [12, 13], oblique illumination was used with an angle of incidence  $\gamma = 5^\circ$ . This set-up allowed easy determination of the pattern wavelength  $\Lambda$  from the distances of the fringes.

The pattern decay has been initiated by a practically instantaneous (within  $10 \mu\text{s}$ ) shutting down of the voltage. The process has been monitored by recording the intensity  $I_{-1}(t)$  of the first order fringe  $n = -1$  [14]. From the analysis of the time evolution of  $I_{-1}(t)$ , to be described in the subsequent sections, the decay rates have been extracted.

### III. THEORETICAL ANALYSIS OF THE DECAY PROCESS

We consider the standard configuration of a nematic sandwiched between two plates parallel to the  $x$ - $y$  plane at a distance  $d$  ( $-\frac{d}{2} < z < \frac{d}{2}$ ). We concentrate on the planar

configuration, where in the ground state the director is oriented along the  $x$  axis, i. e. parallel to  $\mathbf{n}_0 = (1, 0, 0)$ . Applying an electric voltage  $U$ , which exceeds slightly the threshold  $U_c$ , a stripe pattern develops. It involves a periodic modulation of  $\mathbf{n}$  with wavenumber  $q$  in the  $\mathbf{n}_0$  direction. The modulations are coupled in a positive feedback to the flow in convection rolls and to the space charge distribution with the same periodicity; all spatial variations are confined to the  $x$ - $z$  plane (normal rolls).  $\mathbf{n}$  is characterized by its space- and time dependent angle,  $\theta^{EC}(x, z, t)$ , with the  $x$ -axis. It is convenient to separate an amplitude  $\theta_m$  and the part periodic along  $x$  from  $\theta^{EC}$ , which is thus presented as  $\theta^{EC}(x, z, t) = \theta_m \sin(qx) \vartheta^{EC}(q, z, t)$  where  $\vartheta^{EC}(q, 0, 0)$  is normalized to one.

The threshold voltage  $U_c$ , the critical wavenumber  $q_c$  of the roll pattern and the director profile  $\vartheta^{EC}(q, z, t)$  can be obtained from a linear stability analysis of the standard model (SM) of EC [7], which consists of a set of coupled partial differential equations (PDE). Galerkin methods [15] are very convenient to obtain numerical solutions of the SM. The various fields (director, flow, charge density) are represented in the form of appropriate series expansions, like

$$\vartheta^{EC}(q, z, t) = \sum_{m=-\infty}^{\infty} e^{im\omega t} \sum_{l=1}^{\infty} a_{ml}(q) \sin\left(l\frac{\pi}{d}\left(z + \frac{d}{2}\right)\right), \quad (1)$$

for the director, which automatically fulfill the boundary conditions of vanishing distortion,  $\vartheta^{EC}(q, \pm\frac{d}{2}, t) = 0$ , at the confining plates. Due to the up-down symmetry of standard EC the solutions are either odd or even against the reflection  $z \rightarrow -z$ . At small dimensionless control parameter values  $\varepsilon = \frac{U^2 - U_c^2}{U_c^2}$ , i.e. near onset,  $\vartheta^{EC}$  is even in  $z$  and thus  $a_{ml}(q) = 0$  for all even values of  $l$ . The solutions are in addition characterized by their parity under the transformation  $t \Rightarrow t + \frac{\pi}{\omega}$ . While  $\vartheta^{EC}$  has even parity ( $a_{ml} = 0$  for odd  $m$ ) in the *conductive* regime, it switches to odd parity in the high-frequency *dielectric* regime ( $a_{ml} = 0$  for even  $m$ ). By projecting the SM equations on the Galerkin modes one arrives at a system of linear equations for the expansion coefficients like the  $a_{ml}(q)$ , which are determined numerically. Truncating at 8 Galerkin modes ( $0 < l < 8$ ) in the  $z$ -direction and at 3 temporal modes ( $0 < |m| < 3$ ) usually gives an excellent description of patterns near onset. For the nematic **Phase 5** the director profile  $\vartheta^{EC}(q, z, t)$  turns out to be dominated by the leading non-vanishing terms, i.e.  $a_{10} \approx 1$  in the conductive regime and  $a_{1\pm 1} \approx \frac{1}{2}$  in the dielectric regime. The other coefficients  $a_{ml}$  yield only small ( $< 5\%$ ) corrections.

The decay of a pattern, which starts when the voltage is suddenly switched off, at  $t = 0$ ,

does not change the wavenumber  $q$ . Therefore we use for the director profile  $\theta^d$  during the decay the representation  $\theta^d(x, z, t) = \theta_m \sin(qx) \vartheta^d(q, z, t)$  in analogy to  $\theta^{EC}(x, z, t)$ . As already mentioned the analysis of the decay process requires the solution of a linear eigenvalue problem, which originates from the standard model, to determine the decay rates  $\mu_k(q)$  and the decay modes  $N_k(q, z)$ . Compared to the analogous calculation of the critical EC values, the equations become simpler [5], since for zero electric field the charge and the director relaxation dynamics are decoupled (see Appendix).

In line with the standard procedure for linear PDEs the time evolution of the decaying director profile  $\vartheta^d(q, z, t)$  can be represented as:

$$\vartheta^d(q, z, t) = \sum_{k=1}^{\infty} e^{-\mu_k(q)t} w_k(q) N_k(q, z). \quad (2)$$

The expansion coefficients  $w_k(q)$  are determined by a suitable projection on the initial state  $\vartheta^d(q, z, 0) \equiv \vartheta^{EC}(q, z, 0)$ :

$$w_k(q) = \frac{\pi}{d} \int_{-d/2}^{+d/2} \vartheta^{EC}(q, z, 0) N_k^+(q, z) dz \quad k = 1, 2, \dots \quad (3)$$

where the adjoint linear eigenvectors  $N_k^+(q, z)$  of the eigenvalue problem (see Appendix) fulfill the ortho-normality condition:

$$\frac{\pi}{d} \int_{-d/2}^{+d/2} N_k(q, z) N_l^+(q, z) dz = \delta_{kl} \quad k, l = 1, 2. \quad (4)$$

with the Kronecker symbol  $\delta_{kl}$ .

The expansion coefficients  $w_k(q)$  depend strongly on  $q$ . This is obvious when inspecting their  $q$ -dependence plotted as a function of the dimensionless wavenumber square  $q'^2 = (\frac{qd}{\pi})^2$  in Figs. 3a and 3b for  $k = 1, \dots, 8$ . The  $w_k$  have been determined with the help of Eq. (3), where for simplicity  $\vartheta^{EC}(q, z, 0)$  has been approximated by its leading term  $\sin(\frac{\pi}{d}(z + \frac{d}{2}))$  in Eq. (1). The functions  $w_k(q)$  are very small everywhere except over a certain  $q'^2$  interval, where they rise steeply to a finite value. In other words the  $q'^2$  axis can be covered by a set of intervals, such that for  $q$ -values in their interior a unique integer  $\bar{k}(q)$  exists, such that  $w_{\bar{k}}(q)$  is dominant. With increasing  $q'^2$  the corresponding  $\bar{k}(q)$  increases monotonously. Only in the vicinity of special  $q'^2$  values, where two neighboring  $w_k(q)$  curves cross, i.e. at the borders of the  $q'^2$  intervals described before, the decay is governed by two comparable decay rates  $\mu_{\bar{k}}$  and  $\mu_{\bar{k}+1}$ .

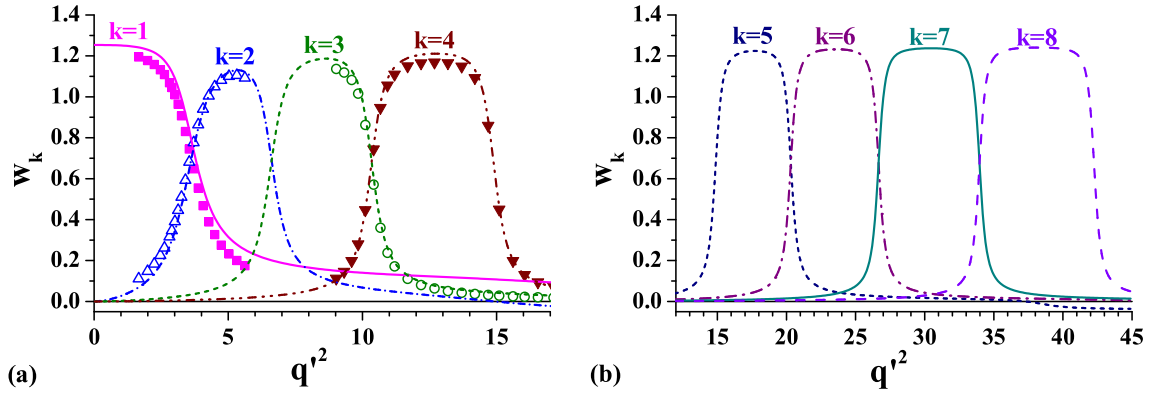


FIG. 3: Variation of the weights  $w_k$  of various decay eigenmodes (plotted with different line styles) with respect to the dimensionless wavenumber square  $q'^2$  for (a)  $k = 1, \dots, 4$  and for (b)  $k = 5, \dots, 8$ , using a  $\sin(\frac{\pi}{d}(z + \frac{d}{2}))$  initial director profile. The weights  $w_k$  calculated from the actual EC director profile are plotted as symbols for a few frequencies in the conductive ( $q'^2 < 6$ , squares for  $k = 1$ , up triangles for  $k = 2$ ) as well as in the dielectric regime ( $q'^2 > 8$ ) (circles for  $k = 3$  and down triangles for  $k = 4$ ).

To test the influence of nonzero coefficients  $a_{ml}$  with  $l > 1$  in Eq. (1) we have calculated for some  $q$  the weights  $w_k(q)$  using the rigorous initial director profile  $\vartheta^{EC}(q, z, 0)$  for Phase 5 in Eq. (3). The corrections are in fact almost negligible (see the symbols in Fig. 3a). Note that for Phase 5 not all  $q$  values can be realized (see Fig. 1b), which explains the missing symbols in the  $6 \lesssim q'^2 \lesssim 9$  interval in Fig. 3a.

#### IV. THEORETICAL DESCRIPTION OF THE DIFFRACTION OPTICS

EC roll patterns represent a periodic spatial modulation of the director which corresponds to an optical phase grating with a lattice constant  $\Lambda$ . This feature allows to keep track of the pattern decay by monitoring the fringe intensities in laser diffraction. Since our director distortions are small, the linearized physical optics approach, discussed in the literature for diffraction from EC rolls [8], is well suited. To disentangle clearly the main contributions to the fringe intensities and to set our notation, we review briefly this previous theoretical approach and allow at the same time for arbitrary profiles  $\vartheta^d(z)$  instead of  $\sin[\frac{\pi}{d}(z + \frac{d}{2})]$  chosen in [8].

The incident light can be well described by a plane wave  $\sim e^{i(\Omega t - \mathbf{k}_0 \mathbf{x})}$ , since the spatial extension of the beam is much larger than  $\Lambda$ . The wave vector  $\mathbf{k}_0$  ( $k_0 = \frac{\Omega}{c}$ ) and the (extraordinary) light polarization are restricted to the  $x$ - $z$  plane.

The optical properties of the nematic are governed by the anisotropic dielectric permittivities  $\epsilon_{\parallel}, \epsilon_{\perp}$  (at the optical frequency  $\Omega$ ) or by the corresponding refractive indices,  $n_e^2 = \epsilon_{\parallel}, n_o^2 = \epsilon_{\perp}$ .

In the case of small distortions of the planar geometry, i.e. for small  $\theta_m$ , the diffraction pattern is determined only by the phase  $k_0 \Phi$  of the transmitted light. Thus an eikonal type approximation for the electric and magnetic field components of the light wave is appropriate. According to [8] in the present geometry the Maxwell equations can be reduced to an equation for the  $y$  component of the magnetic field,  $\mathbf{B}_y$ , of the laser beam. The resulting equation is solved by the substitution:

$$B_y(x, z) = C e^{i(\omega t + k_0 \Phi)} \quad (5)$$

with

$$\Phi(x, z) = x \sin \gamma - n_f z + \beta \theta_m u(x, z). \quad (6)$$

Here  $C$  is a constant and the following abbreviations are used :

$$n_f = n_e \sqrt{1 - \frac{\sin^2 \gamma}{n_o^2}}, \quad \beta = \frac{n_e^2}{n_o^2} - 1. \quad (7)$$

Obviously the function  $u(x, z)$  describes the modification of a plane wave due to the presence of the periodic director distortion. It is useful to separate  $u(x, z)$  as

$$u(x, z) = g_1(z) e^{-iqx} + g_2(z) e^{iqx} \quad (8)$$

which eventually leads to a linear inhomogeneous ordinary differential equation (ODE) for  $g_1(z)$ :

$$\begin{aligned} & \left( -\frac{n_e^2}{n_o^2} q^2 + \partial_{zz} \right) g_1(z) - 2ik_0 [n_f \partial_z g_1(z) + \frac{n_e^2}{n_o^2} iq \sin \gamma g_1(z)] \\ & = [-2k_0 n_f \sin \gamma \vartheta(z) - i \sin \gamma \partial_z \vartheta(z) + q n_f \vartheta(z)] / 2 \end{aligned} \quad (9)$$

The corresponding ODE for  $g_2(z)$  is obtained by the replacement  $q \rightarrow -q$ . The standard matching conditions of the light wave at the boundaries of the cell at  $z = \pm \frac{d}{2}$  are fulfilled if

the following conditions hold:

$$\begin{aligned} g_1\left(-\frac{d}{2}\right) &= \partial_z g_1\left(-\frac{d}{2}\right) = 0; \\ g_2\left(-\frac{d}{2}\right) &= \partial_z g_2\left(-\frac{d}{2}\right) = 0. \end{aligned} \quad (10)$$

The intensity maxima  $I_n$  of the diffraction patterns correspond to rays which include the angles  $\gamma + \alpha_n$  ( $n = \pm 1, \pm 2, \dots$ ) with the  $z$  axis and fulfill the relation

$$\sin(\gamma + \alpha_n) - \sin(\gamma) = \frac{n\lambda}{\Lambda} \quad (11)$$

where  $\alpha_n < 0$  for negative  $n$ . In this paper we concentrate on the intensity  $I_{-1}$  of the first order fringe  $n = -1$  (see Fig. 2). It can be shown by expanding Eq. (5) with respect to  $\theta_m \ll 1$  (see [9]), that within our linear approximation scheme  $I_{-1}$  is given as;

$$I_{-1} = \theta_m^2 |ik_0 g_1\left(\frac{d}{2}\right)|^2 := \theta_m^2 |H_1|^2, \quad (12)$$

where the intensity  $I_0$  of the undistorted laser beam is normalized to one.

We solve Eq. (9) using the 'variation of constant' method. The two linearly independent solutions of the homogeneous equation are given as  $f_{\pm}(z) = e^{i\kappa_{\pm}z}$  with

$$\kappa_{\pm} = n_f k_0 \left[ 1 \pm \left( 1 - R^{-2} \frac{n_e^2 [1 - 2R \sin \gamma]}{n_o^2 n_f^2} \right)^{1/2} \right] \quad (13)$$

and  $R = \frac{k_0}{q}$ . Corrections to geometrical optics and thus diffraction intensities become smaller with increasing  $R$ , which varies between 4 and 73 in our experiments.

The solution of Eq. (9) with the boundary conditions Eq. (10) is then determined as:

$$g_1(z) = \int_{-d/2}^z \frac{f_+(z-z') - f_-(z-z')}{i(\kappa_+ - \kappa_-)} \text{Inh}(z') dz' \quad (14)$$

where  $\text{Inh}(z)$  denotes the inhomogeneity (the right hand side) of the ODE in Eq. (9). It is obvious that the contribution from  $f_+(z)$  - which oscillates strongly on the scale of  $d$  due to  $\kappa_+ \gg \kappa_-$  - can be safely neglected in the sequel. Thus  $I_{-1}$  in Eq. (12) is eventually determined by the following final expression for  $H_1$ :

$$H_1 = -(\bar{c}_1 + \bar{c}_2 \kappa_-) \int_{-1/2}^{1/2} e^{i\kappa_- d(\frac{1}{2} - \bar{z})} \vartheta(\bar{z}) d\bar{z} \quad (15)$$

with

$$\begin{aligned}\bar{c}_1 &= \frac{1}{2}dq n_f \frac{k_0}{(\kappa_+ - \kappa_-)} [1 - 2R \sin \gamma], \\ \bar{c}_2 &= \frac{1}{2}dk_0 \frac{R^{-1}}{(\kappa_+ - \kappa_-)} [R \sin \gamma].\end{aligned}\quad (16)$$

Here we have changed to dimensionless units  $\bar{z} = \frac{z}{d}$ . According to Eq. (15)  $H_1$  appears as a weighted average over the director profile  $\vartheta(z)$ . Note that the contribution  $\propto \bar{c}_2$  originates from a partial integration of the  $\partial_z \vartheta$  term contained in  $Inh(z)$ .

Inspection of Eqs. (12)-(16) insinuates that the diffraction intensity should vary considerably with  $\gamma$ . It follows that even a small non-zero incidence angle, like  $\gamma = 5^\circ$ , is advantageous as seen in the experiment.

Inserting our representation for the decaying director profile given in Eq. (2) into Eq. (15), all integrals can be performed analytically and  $H_1$  appears in a natural way as a sum of the contributions of the different eigenmodes  $N_k(z)$ . Thus eventually the fringe intensity  $I_{-1}$  is given as:

$$I_{-1} = \theta_m^2 C_q \left| \sum_{k=1}^{\infty} c_k^{opt} w_k e^{-\mu_k t} \right|^2. \quad (17)$$

The coefficient

$$c_k^{opt}(q) = \int_{-1/2}^{1/2} e^{i\kappa_-(q)d(\frac{1}{2}-\bar{z})} N_k(\bar{z}, q) d\bar{z} \quad (18)$$

captures the diffracting efficiency of a given decay mode, while

$$C_q = |(\bar{c}_1 + \bar{c}_2 \kappa_-)|^2 \quad (19)$$

is a  $q$  dependent pre-factor.

In Fig. 4 we show a few coefficients  $c_k^{opt}(q)$  ( $k = 1, \dots, 3$ ) calculated for Phase 5 as a function of  $q'^2$  assuming  $\gamma = 5^\circ$ ,  $n_o = 1.558$  and  $n_e = 1.848$  [16]. While  $c_1^{opt}$  decreases with increasing  $q'^2$ , the coefficients  $c_k^{opt}$  for  $k > 1$  show a damped oscillation in the experimentally relevant  $q$  range. In analogy to the maxima of the weights  $|w_k|$  (see Fig. 3a) the leading maxima of  $|c_k^{opt}|$  are continuously shifted with increasing  $k$  toward higher  $q'^2$  values and appear roughly at the same  $q'$  interval with  $k = \bar{k}(q')$  as defined for  $|w_k(q)|$  in Sect. III. Thus via their product in Eq. (17) the mode selection mechanism ( $w_k$ ) and the optical efficiency ( $c_k^{opt}$ ) enhance each other. The products  $w_k(q)c_k^{opt}(q)$  are shown in Figs. 5a and 5b as a function of  $q'^2$ , which are indeed maximal for  $k = \bar{k}(q)$ . Consequently it is obvious

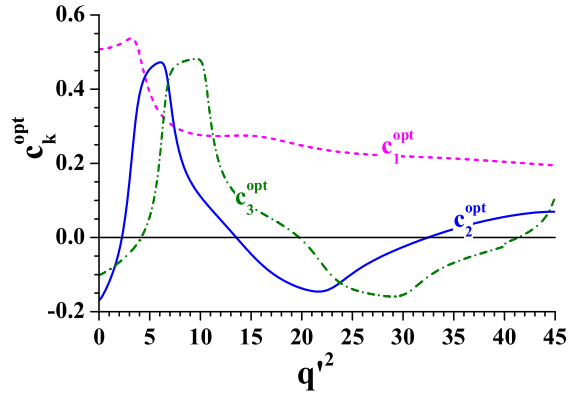


FIG. 4: Variation of the diffraction efficiency of the first ( $c_1^{opt}$ , solid line), the second ( $c_2^{opt}$ , dashed line) and the third ( $c_3^{opt}$ , dotted line) decay eigenmodes as a function of the dimensionless wavenumber square  $q'^2$ .

that the initial stage of the pattern decay, at small  $t$ , is for a given  $q$  governed by the decay rate  $\mu_{\bar{k}}(q)$ . Since  $\bar{k}(q) > 1$  for  $q^2 > 4$ , we would like to emphasize that the initial decay is not automatically governed by the smallest decay rate  $\mu_1(q)$ , as one might have guessed intuitively. With increasing  $t$ , however, we inevitably arrive at a time  $t_1$  where the relation:

$$|c_{\bar{k}}^{opt} w_{\bar{k}}| e^{-\mu_{\bar{k}} t_1} = |c_{\bar{k}-1}^{opt} w_{\bar{k}-1}| e^{-\mu_{\bar{k}-1} t_1} \quad (20)$$

holds and  $\mu_{\bar{k}-1}$  comes into play. Upon further increasing  $t$  one visits all lower  $k$  values until  $k = 1$  is reached. With the analytical expression Eq. (17) at hand there is no difficulty to study the time dependence of  $I_{-1}(t)$  in any detail. On the other hand, when only experimental values for  $I_{-1}(t)$  are given, we are faced with the problem to extract the decay rates  $\mu_k(q)$  in a controlled way.

For that purpose we have produced a set of values of  $I_{-1}(t)$  from Eq. (17) in an interval  $t_a < t < t_a + T_f$ . They are fitted to an exponential curve  $Ae^{-2\mu_f t}$ , where the factor 2 in the exponent is obvious since  $I_{-1}(t)$  depends quadratically on the tilt angle. The interval  $T_f$  has to be chosen small enough, to allow for discriminating the sequence of the dominant  $\mu_k$  which are visited with increasing  $t_a$  according to our general analysis above. As a test we applied the fitting procedure to the analytical expression for  $I_{-1}(t)$  given in Eq. (17). The weights of the decay modes have been calculated from the initial EC state for a number of  $q$  values (including ones from the conductive as well as from the dielectric regime). It is convenient to nondimensionalize the effective exponents using the characteristic director

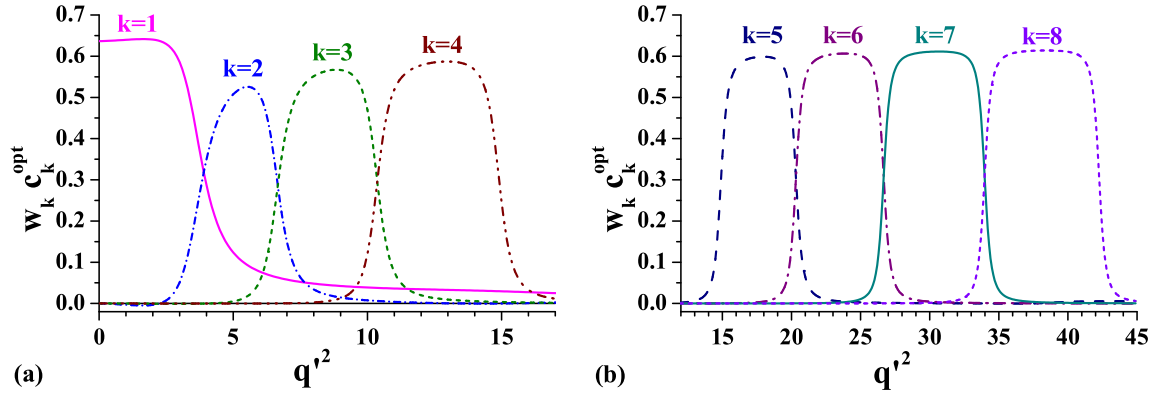


FIG. 5: Contribution of modes to the diffraction intensity  $w_k c_k^{\text{opt}}$  (plotted with different line styles) with respect to the dimensionless wavenumber square  $q'^2$  for a;  $k = 1, \dots, 4$  and for b;  $k = 5, \dots, 8$ , assuming a  $\sin(\frac{\pi}{d}(z + \frac{d}{2}))$  initial director profile.

relaxation time  $\tau_d = \frac{\gamma_1 d^2}{K_1 \pi^2}$  ( $\gamma_1$  is a rotational viscosity,  $K_1$  the splay elastic constant), which is of the order of 0.1 s for  $d = 10 \mu\text{m}$ . The resulting  $\mu'_f = \mu_f \tau_d$  are shown in Fig. 6 together with the first few  $\mu'_k = \mu_k \tau_d$  branches as a function of  $q'^2$ . It is reassuring that our  $\mu'_f$  reproduce the  $\mu'_k = \mu_k \tau_d$  branches very well: the  $\mu'_f$  follow the  $\mu'_k$  branches, and switch to the next,  $\mu'_{k+1}$ , branch with increasing  $q'^2$ . This scenario has already been described when analyzing the experimental data in [5].

In order to have a closer look at the time dependence of the  $I_{-1}(t)$  curves the starting point  $t_a$  of our fitting regime was continuously shifted from  $t_a = 0$  towards larger times. Thus we define an effective decay rate  $\mu'_f(t_a)$ . Figures 7a and 7b exhibit examples of  $\mu'_f(t_a)$  for the conductive ( $q'^2 = 5.619$ ) as well as for the dielectric ( $q'^2 = 18.796$ ) regime, respectively. A gradual crossover from the decay rate of the dominant mode ( $\mu'_f(0) = \mu'_{\bar{k}}$ ) via the intermediate  $\mu'_k(q)$  with  $k < \bar{k}$  toward the slowest decay rate  $\mu'_1$  is clearly identified.

The time evolution of  $\mu'_f(t_a)$  in dependence on the wave number becomes more transparent when they are normalized with respect to their maxima  $\mu'_f(0)$ . The reduced decay rates  $\bar{\mu}'(t_a) = \frac{\mu'_f(t_a)}{\mu'_f(0)}$  are shown in Fig. 8. For the lowest  $q$  the slowest mode  $\mu_1(q)$  is the dominant one, so  $\mu'_f(t_a)$  is practically constant, while for increasing  $q$ , where  $\bar{k}(q) > 1$ , also larger  $\mu_k$  with  $k < \bar{k}$  come into play before the curves saturate again at the slowest mode  $\mu_1$  at  $t_a \gtrsim \frac{15}{\mu'_{\bar{k}}}$ . Notice, however, that by this time, the fringe intensity has already decreased by a factor of  $3 \cdot 10^{-7}$  which is much too low to be resolved in the experiment.

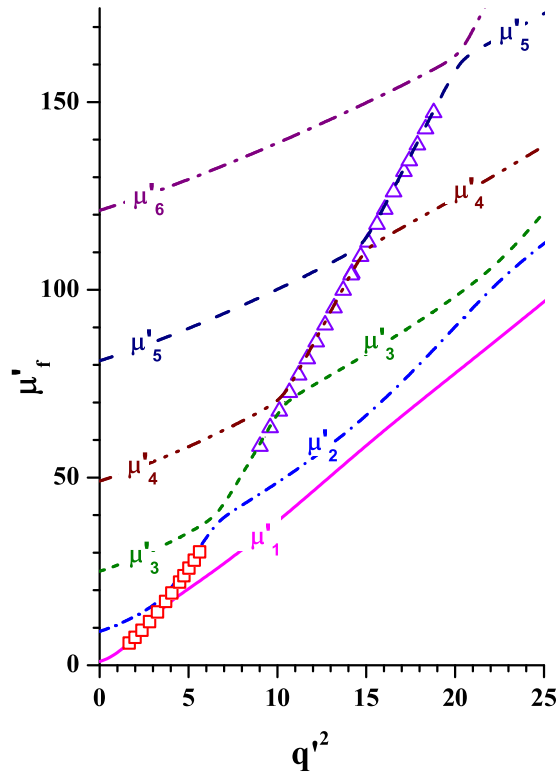


FIG. 6: Dimensionless decay rates  $\mu'_f$  obtained by a single exponential fit versus  $q'^2$  for the start of the decay. Squares and triangles indicate decay of conductive and dielectric rolls, respectively. The lines of different style depict the  $\mu'_1, \dots, \mu'_7$  branches of the dispersion relation.

For completeness we have also plotted the mode independent normalization factor  $C_q$  as a function of  $q'^2$  in Fig. 9, which determines the absolute intensity  $I_{-1}$  of the first order fringe  $n = -1$ . It becomes fairly small at large  $q^2$  and approaches zero at a certain  $\gamma$ -dependent wavenumber  $q_\gamma$ . The absolute intensity, which sets a limitation on resolving the patterns, has otherwise no direct relevance for the determination of the decay rates. In addition we have no real access to the initial amplitude  $\theta_m$  in Eq. (17) which determines the fringe intensity as well.

## V. COMPARISON WITH EXPERIMENTS

To compare experiments directly with theory we have first analyzed the decay of initial small-amplitude roll patterns, that have been prepared with applied voltages slightly above

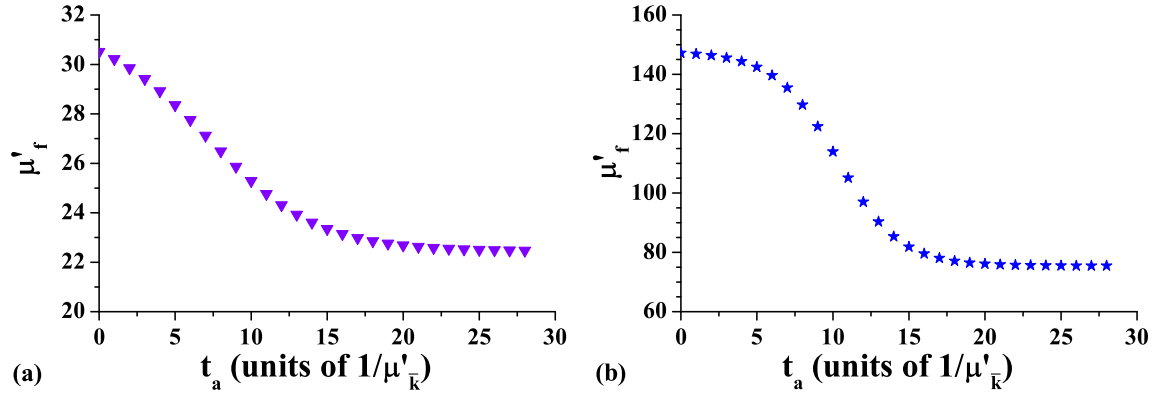


FIG. 7: Dimensionless decay rates  $\mu'_f$  obtained by a single exponential fit versus the time  $t_a$  elapsed between switching off the voltage and start of the fit (a) in the conductive regime ( $q'^2 = 5.62$ ,  $\bar{k} = 2$ ,  $\mu'_2 = 31.28$ ,  $\mu'_1 = 22.42$ ), (b) in the dielectric regime ( $q'^2 = 18.80$ ,  $\bar{k} = 5$ ,  $\mu'_5 = 147.64$ ,  $\mu'_4 = 121.23$ ,  $\mu'_3 = 94.27$ ,  $\mu'_2 = 84.10$ ,  $\mu'_1 = 73.21$ ).

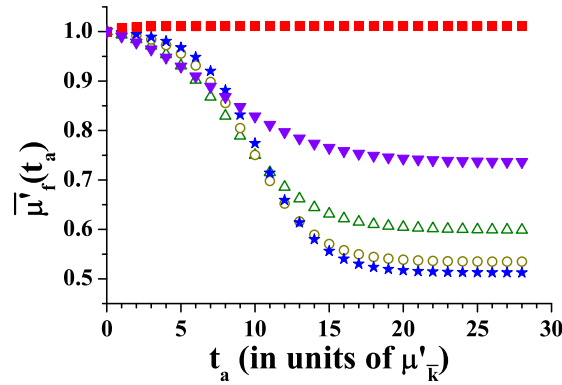


FIG. 8: Temporal evolution of the normalized decay rates  $\bar{\mu}'_f(t_a)$  obtained by a single exponential fit for  $q'^2 = 1.88$  (solid squares),  $q'^2 = 5.62$  (solid up triangles),  $q'^2 = 9.02$  (open up triangles),  $q'^2 = 15.10$  (open circles) and  $q'^2 = 18.80$  (solid stars).

the threshold  $U_c(\omega)$ . In close analogy to our analysis of  $I_{-1}(t)$  in the previous section the experimental fringe intensities have been fitted to an exponential function for different  $q$ . The resulting maximal (dimensionless) decay rates  $\mu'_{exp}$  for  $t_a = 0$  (shown as solid triangles in Figs. 11a and 11b) agree very well with the theoretical ones (i.e. with  $\mu'_{\bar{k}}$ ) as well as with the simulated ones in Fig. 6.

However, since the pattern amplitude becomes too small at a later stage of the decay

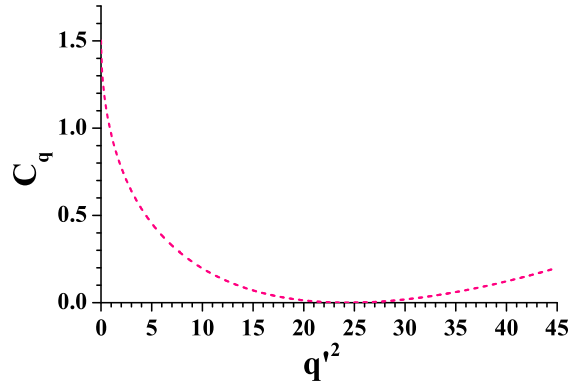


FIG. 9: Variation of  $C_q$  with respect to the dimensionless wavenumber square  $q'^2$ .

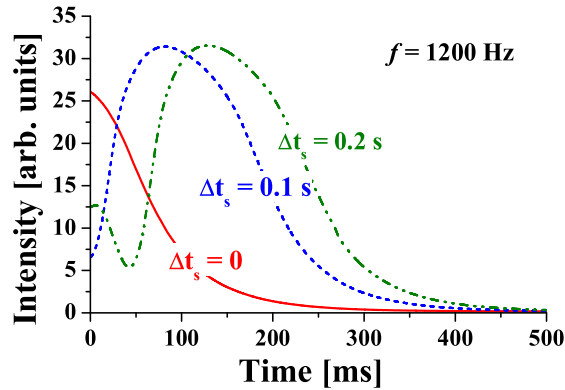


FIG. 10: Temporal evolution of the light intensity of the 1st order diffraction fringe following the shut-down of the applied voltage in a  $28 \mu\text{m}$  thick cell of Phase 5A. Curves with different line styles correspond to different values of the period  $\Delta t_s$  during which an increased amplitude excitation ( $\varepsilon_p = 0.18$  instead of  $\varepsilon = 0.02$ ) was used.

process, it was not possible to reach the further  $\mu_k$  with  $k < \bar{k}$  which must in principle show up (see Fig. 7). Thus we will explore in the following subsections the possibility to initiate the decay process with higher amplitudes and/or with different driving waveforms and thus to modify the initial conditions. We suspect that then the  $z$ -profile of the director in the EC state could experience a considerable modification, which is expected to affect the  $w_k(q)$  functions, such that the  $\mu_{\bar{k}}$  mode calculated before will not be the dominant one. This in principle could lead to an overall acceleration or slowing down of the decay. Model calculations with (realistically) deformed director profiles showed a slowing down.

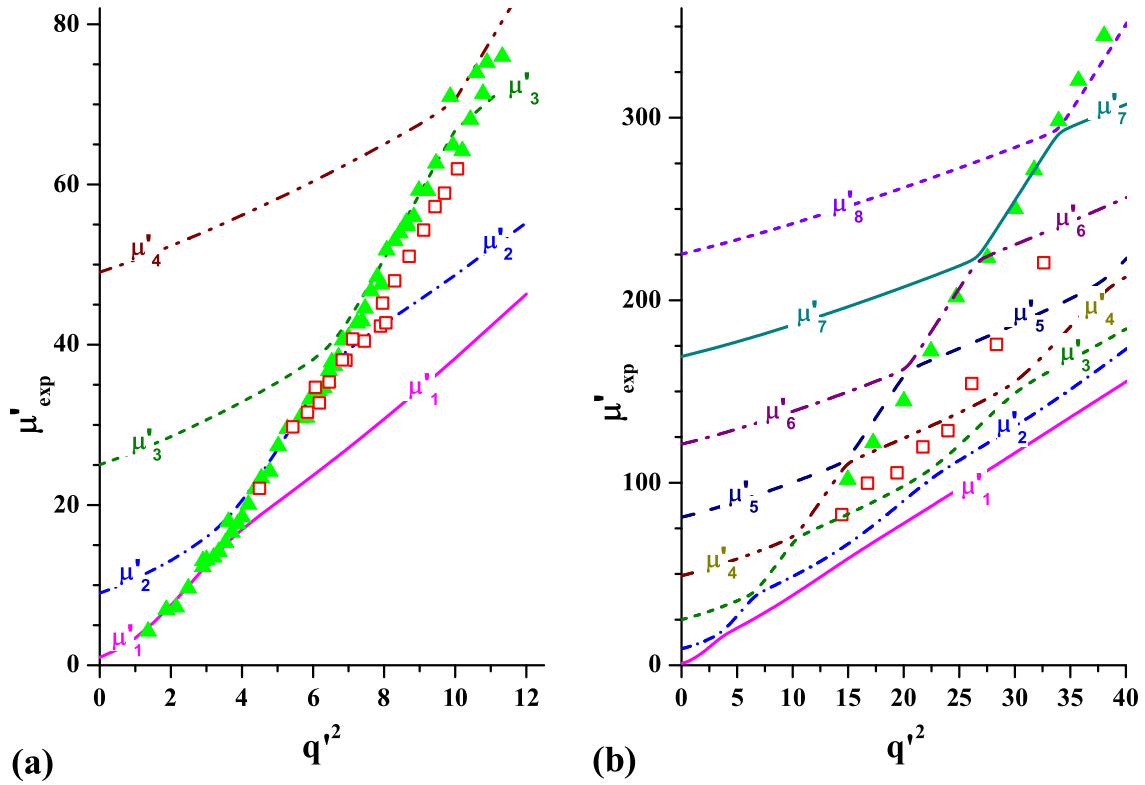


FIG. 11: Theoretical ( $\mu'_k$ ) and measured ( $\mu'_{exp}$ ) values of the dimensionless decay rate of the director versus dimensionless  $q'^2$  for (a) the conductive mode of **Phase 5A**, (b) the dielectric mode of **Phase 5**. Lines of various styles correspond to the eight lowest branches of the dispersion relation. Solid triangles are the data measured at sinusoidal excitation with  $\Delta t_s = 0$ , empty squares are the data obtained at square wave excitation with  $\Delta t_s = 0.2$  s.

### A. Sine wave excitation

Low amplitude initial patterns are typically produced in our experiments by increasing the applied rms voltage  $U$  slowly above the threshold  $U_c$  and waiting some time (of the order of minutes) to allow for equilibration. There is, however, an obstacle to proceed to higher amplitudes  $\theta_m$ : roll patterns become zigzag unstable already very near to threshold ( $\varepsilon \approx 0.04$  [4]). This instability leads to roll pinching, generation of dislocation pairs and thus to defect turbulence, which destroys the homogeneity of the pattern. The resulting diffuse scattering deteriorates the resolution of the diffraction spots and does in practice not allow precise measurements for  $\varepsilon \gtrsim 0.07$ .

Though the growth of the pattern amplitude and the nucleation of defects are both consequences of driving at higher  $\varepsilon$ , the two phenomena do not occur on the same time scale. Defects cause a quite extended distortion of the director and of the flow patterns by phase diffusion, thus the characteristic time for this process is typically longer than that of the simple growth of the amplitude. Therefore, if we just 'kick' the system by applying a higher voltage for a sufficiently small period only, one expects that the system can be driven temporarily above the zigzag destabilization limit to obtain higher pattern amplitude without the appearance of defects and/or the change of  $q$ . Thus we have designed an additional device which has allowed for a fast non-adiabatic amplification of the voltage over a controlled switching period of time  $\Delta t_s = 0 - 1$  s. This technique proved to be indeed efficient, as increasing the voltage by 7.5 % (i.e. jumping from  $\varepsilon = 0.02$  to  $\varepsilon_p \approx 0.18$ ) for  $\Delta t_s = 0.2$  s the number of visible diffraction orders  $n$  (note that  $I_n \propto \theta_m^{2n}$  [8, 13]) could be temporarily doubled without noticeable increase in scattering. We have found that larger jumps in the applied voltage, have to be associated with shorter periods  $\Delta t_s$ , if we intend to avoid nucleation of defects (i.e. to preserve the sharpness of the fringes). The decay curves for different switching times  $\Delta t_s$  are shown in Fig. 10. In contrast to the monotonous decay for  $\Delta t_s = 0$ , from which we extract the decay rates  $\mu_{\bar{k}}$ , the presence of minima and maxima in the  $I_{-1}(t)$  curves recorded at larger  $\Delta t_s$  indicate much bigger initial pattern amplitudes  $\theta_m$ . At larger amplitude  $\theta_m$  one leaves the linear regime and both amplitude- and phase grating effects of the periodic director modulations have to be considered. According to the literature ([12, 13]) the fringe intensity  $I_{-1}$  is then given as:

$$I_{-1} \propto \left[ J_1(Q\vartheta_m) \right]^2. \quad (21)$$

Here  $Q$  is a factor depending on the material parameters and the angle of incidence and  $J_1$  denotes the Bessel function of order 1. The oscillatory behavior of  $J_1$  provides a natural explanation for the non-monotonous  $\Delta t_s$ -dependence of the decay curves. It is clear that with increasing  $\Delta t_s$  we reach larger  $\theta_m$  for the same  $\varepsilon_p$ , which is reflected in more oscillations of  $J_1$ . The detailed analysis of the decay curves at finite  $\Delta t_s$  is, however, outside the scope of the present paper.

For finite  $\Delta t_s$  it is reasonable to assume, that tails of the  $I(t)$  curves in Fig. 10 which monotonously decay in time, will represent the linear  $\theta_m$  regime which allows to extract the linear decay rate spectrum. It turned out that the resulting  $\mu'_{exp}$  (not shown) were only

slightly below the decay rates obtained with  $\Delta t_s = 0$ .

### B. Square wave excitation

The director profile in the EC state is expected to depend also on the driving waveform of the ac voltage. Therefore changing the waveform of the applied voltage from sinusoidal to different ones offers another way to alter the initial conditions.

Thus we have tentatively combined square wave driving with the kicking procedure (a jump from  $\varepsilon \approx 0.02$  to  $\varepsilon_p \approx 0.18$  for  $\Delta t_s = 0.2$  s) described before with the hope to change the initial condition substantially. The decay rates obtained under such conditions are compared in Figs. 11a and 11b with those measured at sinusoidal voltage with  $\Delta t_s = 0$ . It is seen that in the conductive regime (Fig. 11a) the decay rates obtained by the two types of excitation coincide at low  $q'^2$ , as expected. The noticeable, though not fully convincing, shift to lower  $\mu'_{exp}$  (slower decay) at  $q'^2 > 7.3$  may imply that  $\mu(k)(q)$  with  $k < \bar{k}$  have been activated. Deviations are in particular visible in the dielectric regime (see Fig.11b). There the decay rates clearly follow lower decay rate branches  $\mu'_k$  than observed in the low-amplitude, non-kicked case. These observations are in accordance with our expectations that the change of initial conditions have a considerable effect, in particular a decrease of the decay rates. We note that here the system passed a highly nonlinear regime (in analogy to Fig. 10) before arriving at the measured decaying branch. Thus one cannot exclude that according to Eq. (20) the initially dominant mode has not survived in this process, which could also contribute to the shift of the detected decay rates.

## VI. CONCLUSIONS

In this paper we have presented a rigorous analysis of the decay of stripe (roll) patterns in a planar nematic layer, which includes the optical detection of the patterns by diffraction as well. A precise understanding of the selection process of the dominant mode and its decay rate has been achieved. We found that the dominant decay rate can differ substantially from the slowest one. The results have been applied to a standard nematic (Phase 5), where the initial patterns have been generated by electroconvection in the planar configuration. The experimental results are in very good agreement with the quantitative theoretical analysis

in the regime of small director distortions. Some first interesting results for the nonlinear regime and for an ac driving with square waveform need a much more elaborate theoretical analysis, which we plan for the near future.

### Acknowledgments

Financial support by the Hungarian Research Grants No. OTKA-T037336, NKFP-128/6, and the EU Research Training Network PHYNECS and to NATO CRG.LG 973103 is gratefully acknowledged. A.B. and W.P acknowledge support and the hospitality of the Isaac Newton Institute for Mathematical Sciences (Cambridge), where the work has been completed.

- 
- [1] Á. Buka and L. Kramer Eds., *Pattern Formation in Liquid Crystals*, (Springer-Verlag, New York, 1996).
  - [2] T.Börzsönyi, Á.Buka, A.P.Krekhov, and L.Kramer, *Phys.Rev.E.* **58**, 7419 (1998)
  - [3] G. Ahlers, in *Pattern Formation in Liquid Crystals*, edited by Á. Buka and L. Kramer (Springer-Verlag, New York, 1996) p.165.
  - [4] L. Kramer and W. Pesch, in *Pattern Formation in Liquid Crystals*, edited by Á. Buka and L. Kramer (Springer-Verlag, New York, 1996) p.221.
  - [5] N. Éber, S. A. Rozanski, Sz. Németh, Á. Buka, W. Pesch, and L. Kramer, *Phys. Rev. E* **70**, 61706 (2004).
  - [6] S. Chandrasekhar, *Liquid Crystals*, (University Press, Cambridge, 1992).
  - [7] E. Bodenschatz, W. Zimmermann, and L. Kramer, *J. Phys. France* **49**, 1875 (1988).
  - [8] H. M. Zenginoglou, and J. A. Kosmopoulos, *J. Opt. Soc. Am. A* **14**, 669 (1997).
  - [9] H. M. Zenginoglou, and P. L. Papadopoulos, *J. Opt. Soc. Am. A* **18**, 573 (2001).
  - [10] M. Treiber, N. Éber, Á. Buka, and L. Kramer, *J. Phys. II France* **7**, 649 (1997).
  - [11] We have used a standard electronic switch and a high voltage amplifier. Besides a harmonic time dependence we have used in some cases square shape excitation synthesized by a function generator PC card.
  - [12] H. M. Zenginoglou, and J. A. Kosmopoulos, *Appl. Opt.* **27**, 3898 (1988).

- [13] T. John, U. Behn, and R. Stannarius, Eur. Phys. J. B **35**, 267 (2003).
- [14] The intensity  $I_{-1}$  was monitored by an optical fiber connected to a photomultiplier working in its linear regime. Its output was fed through a current-to-voltage converter to either a 16-bit A/D converter card (for measurements in the conductive regime) or to a digital oscilloscope (for measurements in the dielectric regime, where higher sampling rate required to make a compromise with 8-bit resolution)
- [15] see e.g. E. Plaut and W. Pesch, Phys. Rev. E **59**, 1747 (1999).
- [16] F.-D. Hörner, Ph.D. thesis, Universität Bayreuth, Bayreuth, Germany, 1996 (unpublished).

## VII. APPENDIX

In this appendix we sketch briefly the decay of a low-amplitude stripe pattern [5], which is periodic in the  $x$  direction (normal roll). With the help of linearized nematohydrodynamics one arrives at two coupled PDEs for the tilt angle of the director,  $\vartheta(x, z, t) \approx n_z(x, z, t) = N_z(z)\sin(qx)e^{-\mu t}$  and the  $z$ - component,  $v_z(x, z, t) = V_z(z)\cos(qx)e^{-\mu t}$ , of the velocity field:

$$[-\mu' + K'_{33}q'^2 - \partial_{z'}^2]q'\gamma_1 N_z(z') - [\alpha_2 q'^2 + \alpha_3 \partial_{z'}^2]V'_z(z') = 0, \quad (22)$$

$$-[\alpha_2 q'^2 + \alpha_3 \partial_{z'}^2]q'\mu' N_z(z') - [\eta_2 \partial_{z'}^4 - \eta_r q'^2 \partial_{z'}^2 + \eta_1 q'^4]V'_z(z') = 0, \quad (23)$$

Here we have switched to dimensionless quantities marked by primes. The unit of length is chosen as  $\frac{d}{\pi}$ , time is measured in units of the director relaxation time  $\tau_d = \frac{\gamma_1 d^2}{K_{11} \pi^2}$  with the rotational viscosity  $\gamma_1$  and  $K_{11}$  the splay elastic constant.  $K'_{33} = \frac{K_{33}}{K_{11}}$  is the ratio of the bend and splay elastic moduli. The quantities

$$\begin{aligned} \eta_1 &= \frac{1}{2}(-\alpha_2 + \alpha_4 + \alpha_5) ; \quad \eta_2 = \frac{1}{2}(\alpha_3 + \alpha_4 + \alpha_6) ; \\ \eta_r &= \eta_1 + \eta_2 + \alpha_1 \end{aligned} \quad (24)$$

denote the effective (Miesowicz) shear viscosities expressed by the Leslie coefficients  $\alpha_i$ . Furthermore we use realistic rigid boundary conditions, i.e. strong planar anchoring of the director and no slip for the velocities at the bounding plates at  $z' = \pm \frac{\pi}{2}$  in dimensionless units:

$$N_z = 0, \quad V'_z = 0, \quad \partial_{z'} V'_z = 0 \quad \text{at} \quad z' = \pm \frac{\pi}{2}. \quad (25)$$

Eliminating  $V'_z$  and looking for solutions  $N_z(z) \propto e^{isz'}$  one arrives at the following dispersion relation:

$$(\alpha_2 q'^2 - \alpha_3 s^2)^2 \mu' + \gamma_1 (\eta_2 s^4 + \eta_r q'^2 s^2 + \eta_1 q'^4) (K'_{33} q'^2 + s^2 - \mu') = 0. \quad (26)$$

Eq. (26) is cubic in  $s^2$  and has three roots ( $s_1^2$ ,  $s_2^2$  and  $s_3^2$ ). Thus the corresponding eigenvector is constructed as a superposition of three modes:

$$\begin{aligned} N_z(z) &= \sum_{j=1}^3 A_j G_j \cos(s_j z'); \\ V'_z(z) &= \sum_{j=1}^3 A_j \cos(s_j z') \end{aligned} \quad (27)$$

with

$$G_j = \frac{\alpha_2 q'^2 - \alpha_3 s_j^2}{q' \gamma_1 (K'_{33} q'^2 + s_j^2 - \mu')}. \quad (28)$$

The corresponding eigenmodes with odd  $z$ -symmetry are not relevant in our context, since the initial state is always even in  $z$ . The boundary conditions in Eq. (25) single out a discrete eigenvalue spectrum  $\mu'_i$ , with the relevant eigenvectors  $N_i(z')$ ,  $V'_i(z')$  to be calculated from Eq. (27). The eigenvectors are normalized as follows

$$\int_{-\pi/2}^{\pi/2} N_i(z') N_i(z') dz' = 1 \quad (29)$$

fulfilled.

The eigenvalue problem originating from Eqs. (22) and (23) can be symbolically rewritten as:

$$\mathcal{L} \mathbf{W}_i = \mu'_i \mathcal{D} \mathbf{W}_i \quad (30)$$

with the eigenvector  $\mathbf{W}_i := (N_i(z'), V'_i(z'))$ . Furthermore two matrix differential operators  $\mathcal{L}$ ,  $\mathcal{D}$  have been introduced, whose elements can be immediately read off from Eqs. (22) and (23):

$$\begin{aligned} \mathcal{L}_{11} &= [K'_{33} q'^2 - \partial_{z'}^2] q'; & \mathcal{L}_{12} &= -\frac{1}{\gamma_1} [\alpha_2 q'^2 + \alpha_3 \partial_{z'}^2]; \\ \mathcal{L}_{22} &= \mathcal{L}_{12}^2 - \frac{1}{\gamma_1} [\eta_2 \partial_{z'}^4 - \eta_r q'^2 \partial_{z'}^2 + \eta_1 q'^4]; \\ \mathcal{L}_{21} &= \mathcal{L}_{11} \mathcal{L}_{12}; \end{aligned} \quad (31)$$

and

$$\mathcal{D}_{11} = q'; \quad \mathcal{D}_{12} = 0; \quad \mathcal{D}_{21} = 0; \quad \mathcal{D}_{22} = 0. \quad (32)$$

Defining the adjoint operator  $\mathcal{L}^+$  (and similarly  $\mathcal{D}^+$ ) by the identity

$$\int_{-\pi/2}^{\pi/2} \mathbf{U} \mathcal{L} \mathbf{W} dz' = \int_{-\pi/2}^{\pi/2} (\mathcal{L}^+ \mathbf{U}) \mathbf{W} dz' \quad (33)$$

one arrives at the adjoint problem:

$$\mathcal{L}^+ \mathbf{U} = \mu' \mathcal{D}^+ \mathbf{U} \quad (34)$$

The adjoint operator  $\mathcal{L}^+$  can be constructed by partial integration of the left hand side of Eq. (33). It follows that  $\mathcal{L}_{ij}^+ = \mathcal{L}_{ji}$  holds if the boundary terms introduced by partial integration are forced to disappear with a proper choice of the boundary conditions for the adjoint problem:

$$N_z^+ - \frac{\alpha_3}{\gamma_1} \partial_z^2 V_z'^+ = 0, \quad V_z'^+ = 0, \quad \partial_z V_z'^+ = 0 \quad \text{at} \quad z' = \pm\pi/2. \quad (35)$$

Trivially  $\mathcal{D}^+ = \mathcal{D}$  holds as well.

It is now easy to see, that the eigenvalue spectra  $\mu'_i$  of the adjoint and the direct problem (with eigenvectors  $\mathbf{U}_i = (N_i^+(z'), V_i'^+(z'))$  and  $\mathbf{W}_i$ , respectively), coincide. In addition the following orthogonality conditions hold:

$$\frac{1}{q'} \int_{-\pi/2}^{\pi/2} \mathbf{U}_i \mathcal{D} \mathbf{W}_j dz' = \delta_{ij} I_{ii} \quad (36)$$

with

$$I_{ii} = \frac{1}{q'} \int_{-\pi/2}^{\pi/2} \mathbf{U}_i \mathcal{D} \mathbf{W}_i dz' \quad (37)$$

Combining Eqs. (33) and (32) the velocity components drop out and we arrive at the orthogonality relation

$$\int_{-\pi/2}^{\pi/2} N_i^+(z') N_j(z') dz' = \delta_{ij} \quad (38)$$

where we use the convention  $I_{ii} = 1$  in Eq. (37) by a proper normalization of the adjoint eigenvectors. Eq. (38) leads directly to Eq. (4) if we return to physical units.